

Article

The Effect of Gold Nanoparticles on the Catalytic Activity of NiTiO₃ for Hydrodeoxygenation of Guaiacol

Bin Zhao ¹, Guanghui Zhang ¹, Jingbo Mao ², Yanli Wang ¹, Hong Yang ^{3,*} and Xinwen Guo ^{1,*}

¹ State Key Laboratory of Fine Chemicals, PSU-DUT Joint Center for Energy Research Institution, School of Chemical Engineering, Dalian University of Technology, Dalian 116024, China; zhaobingz2008@163.com (B.Z.); gzhang@dlut.edu.cn (G.Z.); wangyanli074@163.com (Y.W.)

² School of Environmental and Chemical Engineering, Dalian University, Dalian 116622, China; james_mao@yeah.net

³ Department of Mechanical Engineering, Faculty of Engineering and Mathematical Sciences, The University of Western Australia, Perth, WA 6009, Australia

* Correspondence: hong.yang@uwa.edu.au (H.Y.); guoxw@dlut.edu.cn (X.G.)

Abstract: Guaiacol is a typical model compound used to investigate and understand the hydrodeoxygenation behaviour of bio-oils, which is critical to their application as an alternative to fossil resources. While extensive research has been carried out on developing catalysts for guaiacol hydrodeoxygenation, the true active sites in these catalysts are often illusive. This study investigated the effect of Au-loading on the catalytic activity of NiTiO₃ for the hydrodeoxygenation of guaiacol. It showed that metallic Ni formed by the partial reduction in NiTiO₃ was responsible for its catalytic activity. Au-loading in NiTiO₃ effectively reduces the temperature required for the NiTiO₃ reduction from 400 °C to 300 °C. Consequently, at an Au-loading of 0.86 wt%, the 0.86 Au/NiTiO₃-300 °C catalyst was found to deliver a guaiacol conversion of ~32%, more than 6 times higher than that of the pure NiTiO₃-300 °C catalyst.

Keywords: hydrodeoxygenation; reduction; Au/NiTiO₃; guaiacol; metallic Ni



Citation: Zhao, B.; Zhang, G.; Mao, J.; Wang, Y.; Yang, H.; Guo, X. The Effect of Gold Nanoparticles on the Catalytic Activity of NiTiO₃ for Hydrodeoxygenation of Guaiacol. *Catalysts* **2021**, *11*, 994. <https://doi.org/10.3390/catal11080994>

Academic Editors: Yinghong Yue and Hong Du

Received: 24 July 2021

Accepted: 16 August 2021

Published: 19 August 2021

Publisher's Note: MDPI stays neutral with regard to jurisdictional claims in published maps and institutional affiliations.



Copyright: © 2021 by the authors. Licensee MDPI, Basel, Switzerland. This article is an open access article distributed under the terms and conditions of the Creative Commons Attribution (CC BY) license (<https://creativecommons.org/licenses/by/4.0/>).

1. Introduction

Lignocellulosic biomass is a good alternative to fossil resources to produce fine chemicals; consequently, it has attracted great attention over the past few decades [1–3]. Conversion of lignin to other chemicals has been widely studied as it is the main component in lignocellulosic materials to produce biobased products [4,5]. Depolymerization of lignin by fast pyrolysis has been reported to produce lignin-derived bio-oil [6–9]. This bio-oil is typically a complex mixture of various oxygenated organic compounds of low molecular weights, such as phenolic monomers, dimers and oligomers [10]. This abundance of oxygenated compounds in the bio-oil causes high thermal instability, which limits its wide-spread utilizations [11]. Catalytic hydrodeoxygenation is considered the most efficient method to reduce oxygen contents in the bio-oil, thus produce the so-called upgraded bio-oil [12].

To understand the hydrodeoxygenation behaviour of the lignin-derived bio-oils, guaiacol (2-methoxyphenol), as one of the most abundant products from the lignin depolymerization processes, has been used as a model compound and extensively studied [13]. Supported metal catalysts are frequently used in the hydrodeoxygenation of guaiacol to produce saturated hydrocarbons, due to the diverse functions provided by inherent and synergistic properties of metal and supported components [14]. It is reported that many metallic components in the catalyst, including Ni [15–17], Co [18], Fe [19,20], Pt [21,22], Pd [23–25], and Ru [26,27], are highly reactive to guaiacol hydrodeoxygenation. Among them, cost-effective Ni is the preferable active metallic component due to its good catalytic activity [28]. One of the most essential functions of the support in the supported metal catalysts is to disperse metallic particles (often nanoparticles) and prevent their aggregation in catalyst preparation, pre-treatment and reaction.

The support itself could also be catalytically active. With proper design, synergistic metal-support interaction could further enhance the catalytic activity of the designed catalyst. For example, Song et al. [29] studied the HZSM-5 supported Ni catalyst in guaiacol hydrodeoxygenation. They found that the hydrodeoxygenation of guaiacol occurred via multiple steps. Essentially, guaiacol hydrogenated to produce catechol and 2-methoxycyclohexanol by metallic Ni, and then further hydrodeoxygenation occurred on the acid site of the support and metallic Ni. The acid sites from the HZSM-5 support in the vicinity of Ni noticeably increased the activities of Ni by a synergistic action. It is reported by Lai et al. [30] that silica alumina supported Ni catalysts were applied to the hydrodeoxygenation of guaiacol. Guaiacol conversion reached about 30% at 450 °C for 6 h. At the same time, the catalyst was also pretreated at high temperature (450 °C) in pure hydrogen before the reaction, which is energy-consuming and risky. Therefore, it is necessary to design and develop a new catalyst for guaiacol hydrodeoxygenation at mild temperature.

Additionally, the introduction of so-called promoter (e.g., Au or Ag particles) in some catalysts enhances their catalytic activity in guaiacol hydrodeoxygenation. For example, it is reported by Mao et al. [31] that pure anatase-TiO₂ delivered only a marginal activity in guaiacol hydrodeoxygenation, but a significantly enhanced activity when it is loaded with Au. While Au itself does not catalyze the hydrodeoxygenation of guaiacol, it provides sites for H₂ dissociation to occur. The dissociated hydrogen readily spills over to reduce the adjacent TiO₂ and this produces the catalytically active oxygen vacancies [32].

At present, the supported metal catalysts are commonly prepared by co-precipitation and impregnation methods, followed by calcination or pre-reduction at elevated temperature. This almost inevitably results in undesired aggregation of the originally well-dispersed and small-sized metal particles, diminishing their activity.

For supported Ni catalysts, the aforementioned problem may be solved by using ilmenite (NiTiO₃) as both the support and Ni source via an in situ partial reduction in the NiTiO₃ to form Ni active sites within the NiTiO₃ support. In this study, NiTiO₃ and Au/NiTiO₃ catalysts were prepared and studied for the hydrodeoxygenation of guaiacol. The effect of Au loading on the performance and active sites of the Au/NiTiO₃ catalyst was investigated.

2. Results and Discussion

2.1. Phase and Morphology of NiTiO₃ and Au/NiTiO₃ Catalysts

Figure 1 shows the XRD patterns of the as-prepared NiTiO₃ and Au/NiTiO₃ powder samples. It is clear that all diffraction peaks can be indexed to the crystalline NiTiO₃ (JCPDS 33-0960) phase [33]. There were no detection of diffraction peaks of other possible impurity phases such as TiO₂ and NiO, indicating the formation of a single NiTiO₃ phase (Figure 1a). It is also evident that no diffraction peaks attributable to Au (JCPDS 04-0784) were observed in the Au loaded 0.26 Au/NiTiO₃ and 0.85 Au/NiTiO₃ samples (Figure 1b).

Figure 2 shows the SEM and TEM images of the as-prepared NiTiO₃ and Au/NiTiO₃ samples. As seen in the SEM images (Figure 2a,b) and TEM image (insert in Figure 2b), the as-prepared NiTiO₃ consists of rods of micron lengths, formed by self-assembled nanocrystals of less than 100 nm. The rods appear to be highly porous.

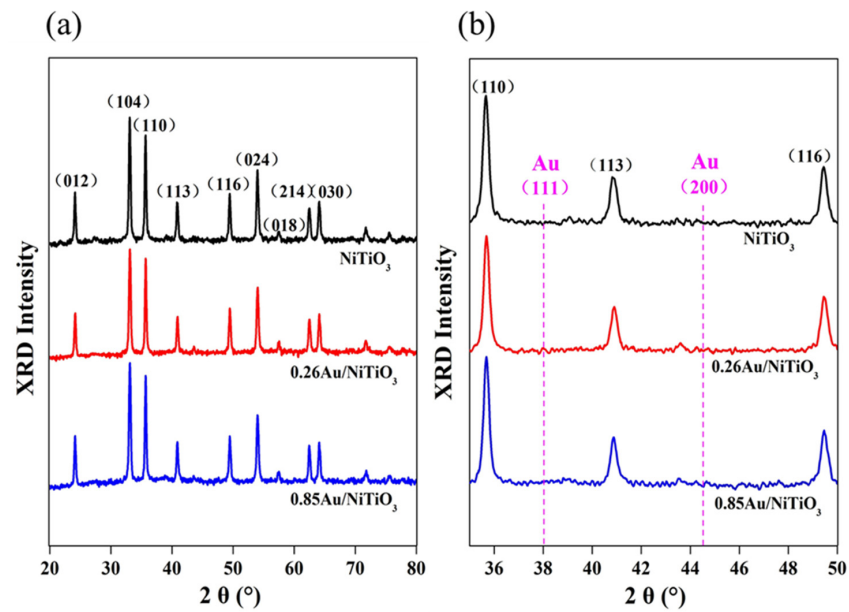


Figure 1. XRD patterns of the as-prepared NiTiO_3 and Au/NiTiO_3 samples obtained at $2\theta = 20\text{--}80^\circ$ (a) and $2\theta = 34\text{--}50^\circ$ (b).

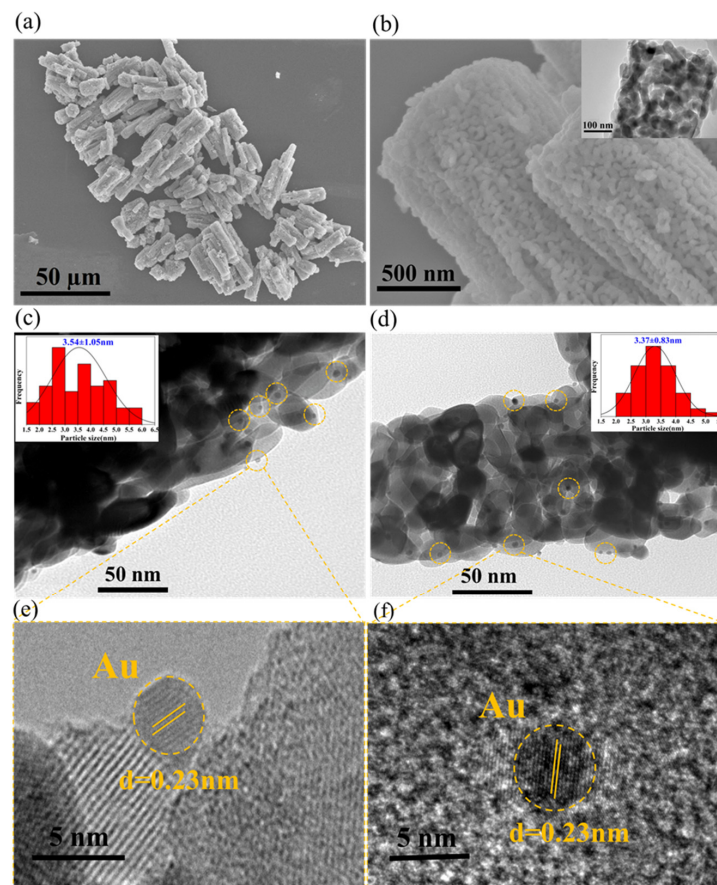


Figure 2. SEM and TEM images of the as-prepared NiTiO_3 sample (a,b). TEM and HRTEM images of 0.26 Au/NiTiO_3 sample (c,e) and 0.85 Au/NiTiO_3 (d,f). The inserts in (c,d) are the Au particle size distributions in the as-prepared 0.26 Au/NiTiO_3 and 0.85 Au/NiTiO_3 samples, respectively.

The general morphology of the Au/NiTiO_3 samples remains very similar to the NiTiO_3 sample. However, when examining closely, tiny particles of Au crystals can be

seen well-dispersed in the two Au-loaded samples, as highlighted in dashed yellow circles (Figure 2d,e). The HRTEM images reveal the highly crystalline nature of the Au particles and lattice d -spacing of $d = 0.23$ nm (Figure 2e,f), consistent with Au(111) [34]. The average sizes of the Au crystals are found to be 3.47 ± 1.12 nm for the 0.26 Au/NiTiO₃ sample (insert in Figure 2c) and 3.37 ± 0.83 nm for the 0.85 Au/NiTiO₃ sample (insert in Figure 2d). The low Au loading, very small crystal sizes and well-dispersed distribution are the likely reasons that Au was not convincingly detected in the XRD analysis of the Au/NiTiO₃ samples.

Table 1 summarizes the measured BET surface areas of the NiTiO₃ and Au/NiTiO₃ samples, as well as the weight percent of Au-loading measured by the ICP. The BET surface area of the samples did not change significantly with the Au-loading. This is consistent with the observation that Au particles are very small of <5 nm and well-dispersed on the surface of NiTiO₃ rods. The Au-loadings determined by the ICP analysis are consistent with the nominal loading of the two samples.

Table 1. BET surfaces areas of the NiTiO₃ and Au/NiTiO₃ samples and Au-loadings measured by ICP analysis.

Sample	BET Surface Area (m ² /g)	Au-Loading (wt%)
NiTiO ₃	26.5	-
0.26 Au/NiTiO ₃	30.9	0.26
0.85 Au/NiTiO ₃	31.9	0.85

2.2. Hydrodeoxygenation of Guaiacol

Figure 3 shows the catalytic performance of NiTiO₃ (Figure 3a) and Au/NiTiO₃ (Figure 3b) obtained under 700 rpm stirring in 3 MPa H₂ at 300 °C for 2 h. The catalysts were subjected to pre-treatment in H₂/He, reducing atmosphere for 1 h at temperatures specified before loaded into the reactor.

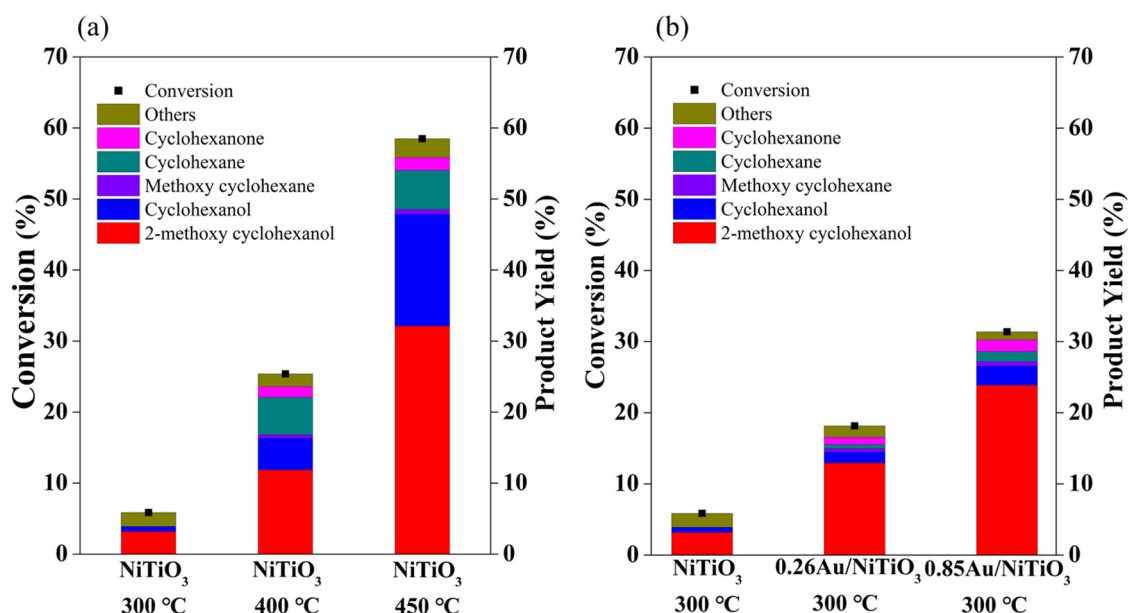


Figure 3. Hydrodeoxygenation of guaiacol obtained under 700 rpm stirring in 3 MPa H₂ at 300 °C for 2 h, over the pure NiTiO₃ pre-treated at 300 °C, 400 °C and 450 °C (a) and over the NiTiO₃ and Au/NiTiO₃ catalysts pre-treated at 300 °C (b).

As seen in Figure 3a, over the pre-treated NiTiO₃-300 °C, the guaiacol conversion was very low (<5%), but increased significantly to ~30% at 400 °C and reached ~58% at 450 °C. The main component in the product is 2-methoxy cyclohexanol and with no phenolic

products detected. Note that “others” in the product yields refer to those not detected by the GC analysis, but deduced from the product mass balance analysis. They are assumed to be mostly C_{8+} and coke formed during the reaction testing.

Compared to the $NiTiO_3$ -300 °C, the $Au/NiTiO_3$ -300 °C (Figure 3b) catalysts showed significantly higher catalytic activities. 0.85 $Au/NiTiO_3$ -300 °C delivered close to 32% guaiacol conversion under the same reaction conditions. In addition, the yield of 2-methoxy cyclohexanol in the products has also increased to 24% as the result of Au-loading.

As reported in a previous study [31], Au-loaded Au/SiO_2 and $Au/Activated\ carbon$ (AC) catalysts delivered very low guaiacol conversions under 6.5 MPa H_2 at 300 °C. In these catalysts, both SiO_2 and AC supports are inactive, thus, the results indicate that Au particles are not catalytically active for the hydrodeoxygenation of guaiacol. If so, what could be responsible for the significantly enhanced activity of Au-loaded $Au/NiTiO_3$ samples?

2.3. The Effect of Au-Loading on the Activity of $NiTiO_3$ Catalysts

Figure 4 shows the Raman spectra of the pre-treated $NiTiO_3$ -300 °C and $Au/NiTiO_3$ -300 °C samples. As seen from the spectrum of the $NiTiO_3$ -300 °C, a series of Raman active modes located between 189 and 770 cm^{-1} are observed, confirming it has a rhombohedral crystalline structure as reported in previous studies [35,36]. The strongest Raman mode at 707 cm^{-1} arises from the symmetric stretching of the TiO_6 octahedral of the $NiTiO_3$ [37]. Evidently, with Au-loading, the overall intensity of the Raman band decreased drastically, especially, for the strongest Raman mode at 707 cm^{-1} . This implies the destruction of TiO_6 units in the $Au/NiTiO_3$ samples.

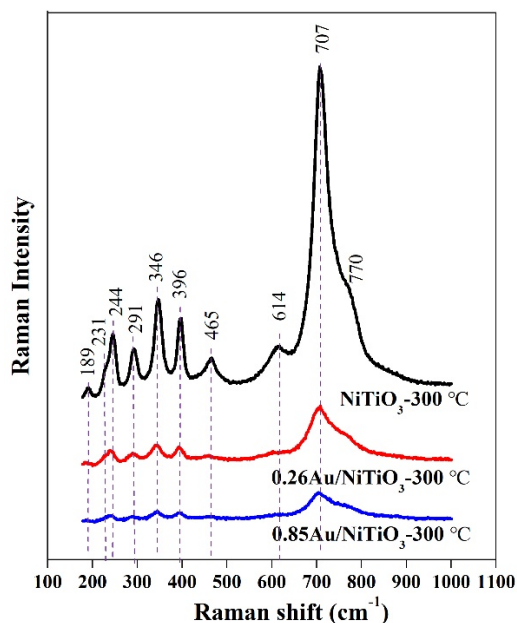


Figure 4. Raman spectra of the $NiTiO_3$ and $Au/NiTiO_3$ samples pre-treated in H_2 at 300 °C.

Figure 5 shows in situ XRD patterns taken for the $NiTiO_3$ and 0.26 $Au/NiTiO_3$ samples held for 0.5 h at each temperature in H_2 (5% H_2/He) from 30 °C to 550 °C. As seen from Figure 5a, the XRD pattern for the pure $NiTiO_3$ (JCPDS 33-0960) sample remains largely unchanged (i.e., the sample remains stable) at below 400 °C. At 400 °C, however, two new diffraction peaks started to emerge at $2\theta = 27.4^\circ$ and 43.1° , attributed to the main diffraction peak of the rutile- TiO_2 and metallic Ni, respectively. The two peaks strengthen progressively with increased reduction temperatures, accompanied by the concurrent reduction in the diffraction intensity of the $NiTiO_3$ phase. By 550 °C, only diffraction peaks associated with the rutile TiO_2 (JCPDS 75-1753) and metallic Ni (JCPDS 01-1258) are observed. Examining the XRD patterns of the 0.26 $Au/NiTiO_3$ sample shown in Figure 5b, they are found to be almost same to those of the pure $NiTiO_3$ sample.

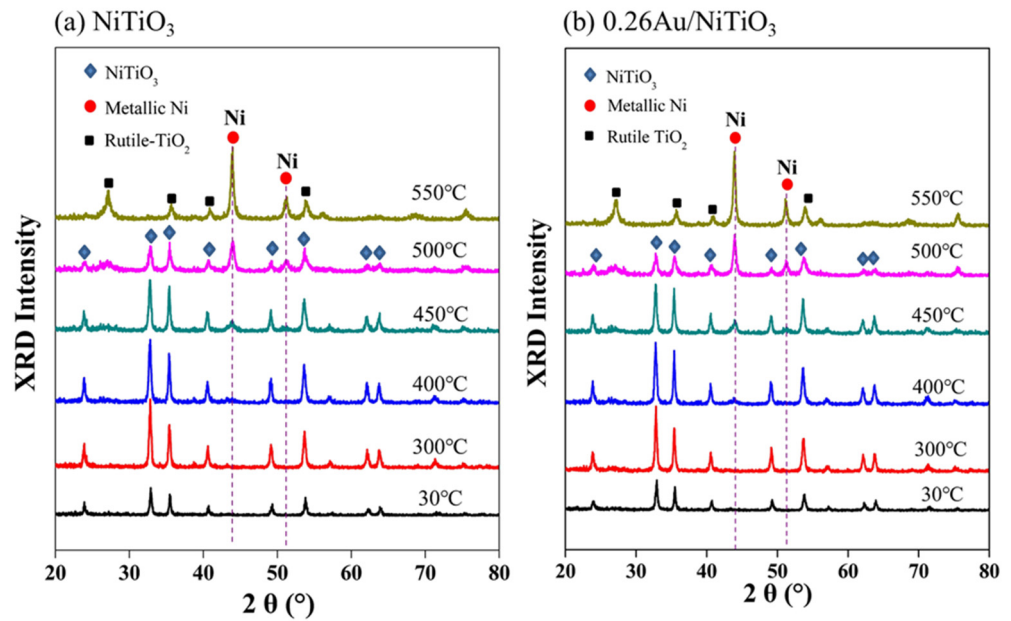


Figure 5. In situ XRD patterns of the NiTiO₃ (a) and 0.26 Au/NiTiO₃ (b) taken at different temperatures in H₂ atmosphere.

Figure 6a shows the DRIFT spectra of CO adsorption taken at 30 °C for the pre-treated NiTiO₃. At 300 °C, only two adsorption bands at ~2175 cm⁻¹ and ~2120 cm⁻¹ are observed on the NiTiO₃-30 °C and NiTiO₃-300 °C samples. They are ascribed to the physically adsorbed CO [38,39]. As the pre-treatment temperature increases to 400 °C, two new bands at ~2053 cm⁻¹ and ~2085 cm⁻¹ appear in the NiTiO₃-400 °C. These two bands are believed to be associated with the chemically adsorbed CO on metallic Ni [40–42]. The intensity of these two bands increases with increased pre-treatment temperature, suggesting an increase in the amount of Ni formed on the NiTiO₃-450 °C.

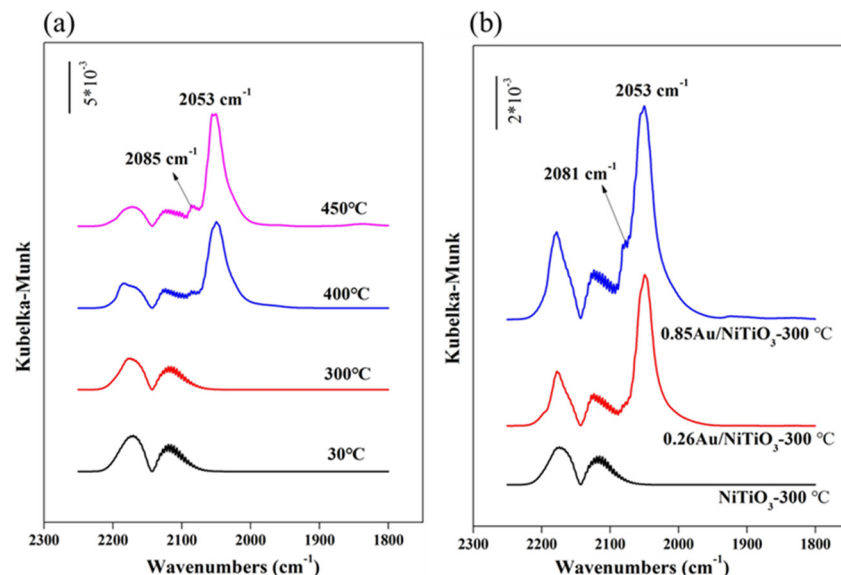


Figure 6. In situ DRIFT spectra of CO adsorptions taken at 30 °C over pre-treated NiTiO₃ at different temperatures (a) and pre-treated NiTiO₃ and Au/NiTiO₃ samples at 300 °C (b).

The results of Raman, in situ XRD and in-situ DRIFT all indicate that the reduction of NiTiO₃ to form metallic Ni has occurred in the reducing atmosphere of H₂. Evidently, loading of Au in these catalysts results in the reduction in the temperature required for the

formation of Ni from 400 °C for the pure NiTiO₃ to 300 °C for the Au/NiTiO₃ samples. This result correlates with the hydrodeoxygenation of guaiacol reaction results presented in Figure 3b, which show a much-enhanced catalytic activity of the Au/NiTiO₃ samples at 300 °C, in contrast to almost no activity of the pure NiTiO₃ sample at the same temperature.

2.4. Effect of Reaction Temperature on Catalytic Performance

Figure 7 summarizes the catalytic performances of the 0.85 Au/NiTiO₃ catalyst at 280 °C, 300 °C, 320 °C and 340 °C. 2-methoxy cyclohexanol is the primary and major product when the reaction was performed at 280 °C and 300 °C. The highest yield of 24% was achieved at 300 °C. When the reaction temperature rises to 340 °C, the yield of cyclohexanol and cyclohexane increases. This is mainly due to the cleavage of C-OCH₃ and C-OH bond in 2-methoxy cyclohexanol at high temperature. According to these results, the increase in reaction temperature only increases the further reaction of 2-methoxy cyclohexanol. Therefore, the temperature of 300 °C was selected for further studies.

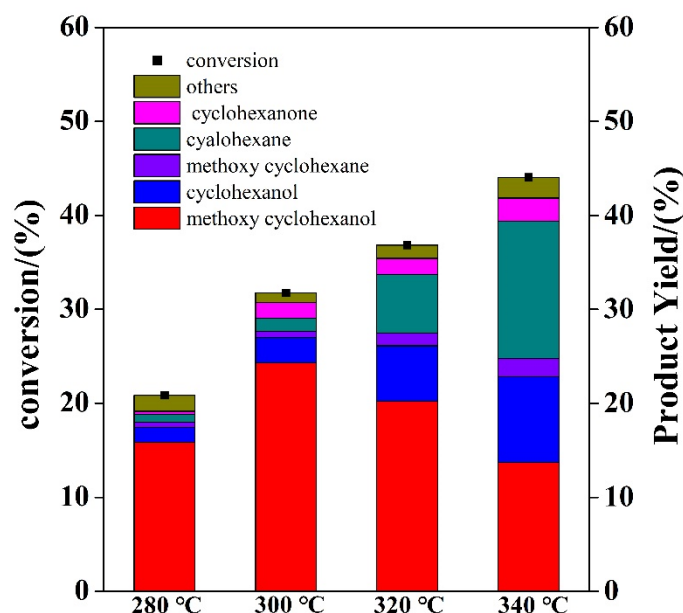


Figure 7. Effect of temperature on guaiacol conversion and product distribution over 0.85 Au/NiTiO₃. Reaction conditions: catalyst 0.2 g, guaiacol 1.30 g, decane 25 mL, P (H₂) = 3 MPa, 300 °C, 700 rpm.

2.5. Catalyst Stability

The stability of the 0.26 Au/NiTiO₃ and 0.85 Au/NiTiO₃ catalysts was performed by three-time recycling experiments in guaiacol hydrodeoxygenation. The recycled catalysts were directly used in the next recycling experiments without any treatment. Figure 8 shows the recycling results of 0.26 Au/NiTiO₃ (Figure 8a) and 0.85 Au/NiTiO₃ (Figure 8b) catalysts. The catalytic performances of the two catalysts are almost same in three consecutive tests, confirming that varying the Au content does not significantly change the catalytic performance.

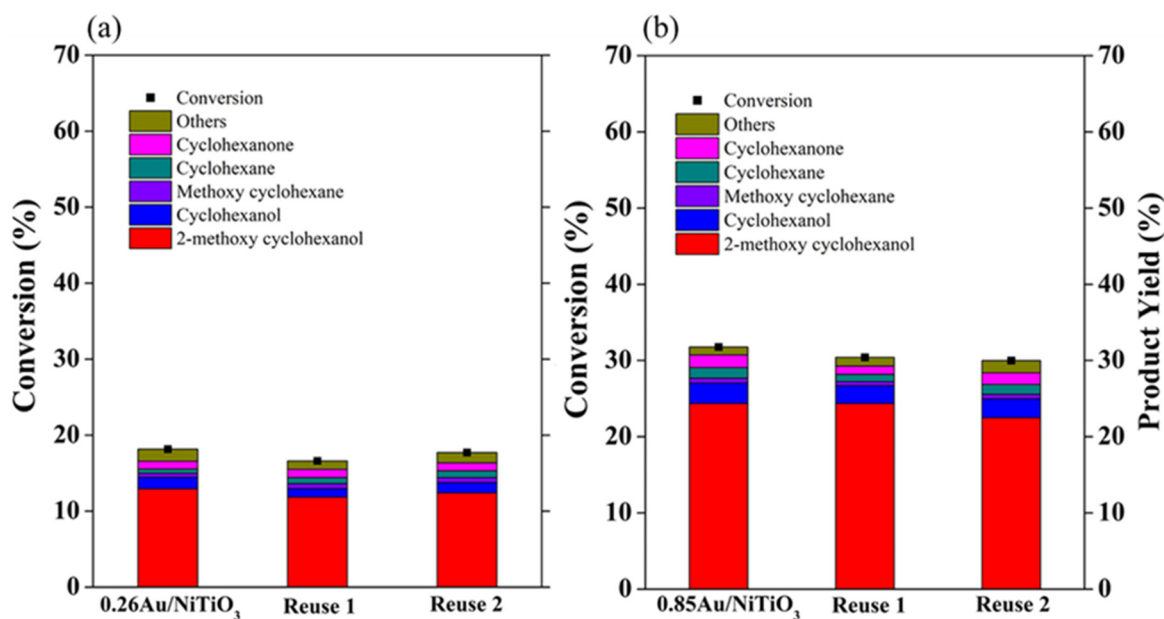


Figure 8. Performance of 0.26 Au/NiTiO₃ (a) and 0.85 Au/NiTiO₃ (b) in three consecutive tests with reuse of the catalysts. Reaction conditions: catalyst 0.2 g, guaiacol 1.30 g, decane 25 mL, P (H₂) = 3 MPa, 300 °C, 700 rpm.

2.6. Discussion

It is well known that supported nickel-based catalysts exhibit high activity for hydrodeoxygenation of guaiacol to saturated products. However, guaiacol hydrodeoxygenation over these catalysts occurred under relatively high reaction temperature. With a monometallic Ni supported on common supports such as Al₂O₃, C and zeolite, the reaction temperature for guaiacol conversion is over 350 °C (Table 2). Forming Ni alloy catalysts on these supports by adding Cu or Pd has been reported but the reaction temperature was almost the same as that of the monometallic Ni catalyst. Moreover, high reduction temperature is needed to activate the Ni catalysts. For example, Zhang et al. [17] found the interaction between NiO and Al₂O₃ resulted in the reduction in NiO at the high temperature (over 600 °C). Hydrogen atoms are the active species to reduce NiO on Ni supported catalysts. Generally, the generation of hydrogen atoms from H₂ molecules have a high energy barrier without catalysts. As for Au/NiTiO₃ catalyst, we use a special support-NiTiO₃, which contains Ni species natively. When Au is supported on NiTiO₃, hydrogen atoms are created by dissociative chemisorption of H₂ molecules on Au surface, and then spill over to the surface of the NiTiO₃, thus decreasing the reduction temperature of Ni²⁺ species to metallic Ni species. In addition, the reaction temperature of guaiacol conversion over Au/NiTiO₃ is lower than that over Ni supported on common supports, which indicates that the metallic Ni species on NiTiO₃ are more active than that on common supports. This may be due to the generation of small Ni cluster at much lower reduction temperature on Au/NiTiO₃. Small Ni cluster will aggregate to Ni particle at high temperature resulting in decreasing catalyst activity.

Table 2. Comparison of Ni-based catalysts for guaiacol conversion.

Catalysts	Feedstock	Reaction Condition			Conversions (%)	Refs
		Temperatures (°C)	Pressure (MPa)	Time (h)		
Ni/C	Guaiacol	350	0.44	3	36	[43]
Ni/MgO	Guaiacol	350	0.44	3	24	[43]
Ni/SiAl	Guaiacol	450	0.1	6	30	[30]
MoO ₃ -NiO/SBA-15	Guaiacol	350	-	8	55	[44]
Ni-Fe/CNTs	Guaiacol	400	3	2	47	[45]
Ni _{36.5} Cu _{2.3} /ZrO ₂ -SiO ₂ -La ₂ O ₃	Guaiacol	360	17	1	~50	[28]
Ni-Pd/SiAl	Guaiacol	450	0.1	6	~28	[30]
Au/NiTiO ₃	Guaiacol	300	3	2	32	This work

3. Experimental

3.1. Catalyst Preparation

The NiTiO₃ nanorods were synthesized following a procedure published in the previous work [33]. Typically, 2.48 g nickel acetate (Damao Chemical Reagent Factory, AR, Tianjin, China) and 3.4 mL tetra-n-butyl titanate (Sinopharm Chemical Reagent Co., Ltd., CP, Shanghai, China) were dissolved in 60 mL ethylene glycol Sinopharm Chemical Reagent Co., Ltd., AR, Shanghai, China) solvent to form a solution (green in colour). The mixed solution was stirred slowly at room temperature for ~10 min resulting in the formation of a brilliant blue precipitate. To ensure a complete reaction of the reagents, the solution was further stirred for 1 h at progressively increased stirring rates. The precipitate was then recovered by centrifugation, carefully washed by ethanol several times, dried in a vacuum oven at 60 °C for 4 h, and finally calcined in air at 600 °C for 2 h to obtain the NiTiO₃ powder.

The Au/NiTiO₃ samples were synthesized by a deposition-precipitation method. Typically, 1 g of NiTiO₃ powder was suspended in a solution of 24.8 mmol L⁻¹ HAuCl₄ 4H₂O (Sinopharm Chemical Reagent Co., Ltd., AR), followed by adjusting the solution to a pH ~7.0 with 0.1 mol L⁻¹ NaOH (Tian Da Chemical Reagent Co., Ltd., AR, Tianjin, China). The solution was stirred vigorously for 4 h at room temperature. Subsequently, the suspension was filtered, extensively washed with deionized water to remove ions, dried at 60 °C for 12 h in vacuum, and finally calcined at 350 °C for 2 h in air to obtain the Au/NiTiO₃ powders. Two Au-loaded NiTiO₃ samples were prepared in this study including 0.26 Au/NiTiO₃ (0.26 wt% Au) and 0.85 Au/NiTiO₃ (0.85 wt% Au).

3.2. Catalyst Characterization

Powder X-ray diffractograms (XRD) of the samples were obtained using a Rigaku SmartLab 9 kW diffractometer (Tokyo, Japan) equipped with Cu K α radiation ($\lambda = 1.5406 \text{ \AA}$), operated at a voltage of 45 kV and a current of 200 mA, and scanned at 2θ from 20° to 80° with a step size of 0.02°. The diffraction data were collected using a PIXcel 1D detector (Tokyo, Japan). In situ XRD patterns were also obtained for catalyst samples at different temperatures (held at each data collection temperature for 0.5 h) between 30 °C to 550 °C in H₂ (5% H₂/He) at a gas flow rate of 30 mL/min. This reduction treatment was performed in a hermetic XRK 900 reactor (Tokyo, Japan) chamber made by Anton Par Corporation. The catalyst powder was packed in a ceramic sample stage with an X-ray transmitting beryllium window. The temperature within the reactor was controlled using a TCU 750 Temperature Control Unit.

The specific surface area (S_{BET}) of the samples was determined by the Brunauer–Emmett–Teller (BET) method from the N₂ adsorption data obtained at 77.3 K using a Micromeritics ASAP 2020 physical adsorption analyzer (Norcross, GA, USA).

Elemental analysis of the samples was carried out using a PerkinElmer Optima 8000 inductively coupled plasma-optical emission spectrometer (ICP-OES) (Shanghai, China).

Scanning electron microscopy (SEM) images were obtained on a cold-field emission Hitachi SU8200 instrument (Tokyo, Japan) with an acceleration voltage of 5 kV. Transmission electron microscopy (TEM) was carried out on a JEM-2100 microscope operated at 200 kV and high-resolution TEM (HRTEM) imaging was obtained on a Tecnai F30 HRTEM instrument (FEI Corp. Portland, OR, USA) operated at 300 kV. The TEM samples were prepared by dropping ethanol suspension of the powder samples on the carbon film-coated copper grids. To prepare for the ethanol suspension, the Au/NiTiO₃ sample was pre-treated at 300 °C in flowing hydrogen for 1 h. The distributions of Au particle size were calculated from the TEM images using Nano Measure 1.2.

In situ DRIFT spectra were carried out in an in situ reaction cell on a Thermo Scientific Nicolet iS50 (Waltham, MA, USA) equipped with an MCT detector. Before CO adsorption, the sample was loaded into the in situ reaction cell and heated in 10% H₂/Ar at 10 °C/min to a set temperature (typically 300 °C) for 1 h. After the treatment, the sample was purged in He and cooled down to 30 °C. The sample was then exposed to 5% CO/He at 30 °C for 3 min and the DRIFT spectrum was recorded after the chemisorption of CO. The DRIFT spectra of the sample were recorded prior to (for the background) and after the CO adsorption and the spectra were obtained as the average of 64 scans at each setting with 4 cm⁻¹ resolution.

UV-Raman spectra were recorded by using a home-made triple-stage UV-Raman spectrograph with a spectral resolution of 2 cm⁻¹. The laser line at 325 nm of an He:Cd laser was used as the exciting source with an output of 30 mW. The laser power at the sample was ~3 mW.

3.3. Catalyst Activity Measurements

Guaiacol hydrodeoxygenation was conducted in a sealed 50 mL stainless-steel batch reactor. Prior to each test, the catalyst sample was pre-treated at 300 °C, 400 °C or 450 °C for 1 h in a flow of 10% H₂/Ar. 1.3 g of guaiacol (Shanghai Mecklin Chemical Reagent Co., Ltd., GC, Shanghai, China) and 25 mL of decane (Tianjin Kemiou Chemical Reagent Co., Ltd., AR, Tianjin, China) and 0.20 g of pre-reduced catalyst was added into the reactor. The reactor was sealed and purged with N₂ for 5 times to remove the air, and then pressurized to 3 MPa H₂. Further, the reactor was heated to 300 °C and kept for 2 h under magnetic stirring at 700 rpm. After the reaction, the reactor was cooled to room temperature. 0.2394 g of n-tetradecane (TCI, GR) as an internal standard and 25 mL of ethanol were loaded into the reactor. The reaction products were qualitatively analyzed using gas chromatography (Agilent 7890A, Wilmington, NC, USA) with a HP-5 column (30 m × 0.32 mm × 0.25 μm) and a flame ionization detector (FID). The identification of reaction products was carried out by GC-MS. All catalysts were repeated at twice. Decane has a high boiling point of 174.2 °C, and the reactants have higher solubility in ethanol, so in this work, Decane was used as a solvent to achieve a high reaction temperature. Ethanol is used to dissolve and dilute the reactants and products for GC analysis after the reaction. n-tetradecane was used as the internal standard for GC analysis.

The conversion of guaiacol (X_{guaiacol} , %) was calculated based on the molar ratio of consumed guaiacol ($n_{\text{consumed guaiacol}}$) to the initial guaiacol in the feed ($n_{\text{initial guaiacol}}$) Equation (1). The product yield (Y_{product} , %) was calculated on basis of the molar ratio of corresponding compounds in the product (n_{compound}) to the consumed guaiacol ($n_{\text{consumed guaiacol}}$) Equation (2).

$$X_{\text{guaiacol}} = \frac{n_{\text{consumed guaiacol}}}{n_{\text{initial guaiacol}}} \times 100\% \quad (1)$$

$$Y_{\text{product}} = \frac{n_{\text{compound}}}{n_{\text{consumed guaiacol}}} \times 100\% \quad (2)$$

4. Conclusions

In summary, the catalytic activity of the NiTiO₃ and Au/NiTiO₃ catalysts and the effect of Au-loading were studied in hydrodeoxygenation of guaiacol to 2-methoxy cyclohexanol. The main conclusions are as following: (1) The activity of the NiTiO₃ and Au/NiTiO₃ catalysts for guaiacol hydrodeoxygenation resulted from the in situ formation of metallic Ni via the reduction in NiTiO₃. (2) Noticeable reduction of pure NiTiO₃ in H₂ only occurs at a temperature of 400 °C and above. However, with Au-loading, the reduction in Au/NiTiO₃ in H₂ starts at a lower temperature of 300 °C. In other words, Au-loading promotes the reduction of NiTiO₃ to form active metallic Ni. (3) The NiTiO₃ catalyst was largely inactive for guaiacol hydrodeoxygenation at 300 °C, but achieved more than 30% guaiacol conversion and higher than 11% 2-methoxy cyclohexanol selectivity at 400 °C. However, the Au-loaded 0.85 Au/NiTiO₃ catalyst delivered similar guaiacol conversion at 300 °C. There are great prospects and challenges in designing Ni catalysts with high catalytic performance for HDO of lignin-derivative oil. High efficiency Ni-based catalysts will promote rapid development of biomass energy. However, Ni-based catalysts are still in the laboratory stage, and it is still a huge challenge to achieve large-scale development and application in biomass upgrading.

Author Contributions: Conceptualization, B.Z. and X.G.; Data curation, bin zhao; Formal analysis, B.Z., G.Z. and J.M.; Investigation, B.Z.; Project administration, X.G.; Writing—original draft, bin zhao; Writing—review & editing, G.Z., Y.W., H.Y. and X.G. All authors have read and agreed to the published version of the manuscript.

Funding: This research received no external funding.

Data Availability Statement: The data are contained within the article.

Conflicts of Interest: The authors declare no conflict of interest.

References

1. Ragauskas, A.J.; Williams, C.K.; Davison, B.H.; Britovsek, G.; Cairney, J.; Eckert, C.A.; Frederick, W.J.; Hallett, J.P.; Leak, D.J.; Liotta, C.L.; et al. The path forward for biofuels and biomaterials. *Science* **2006**, *311*, 484–489. [[CrossRef](#)]
2. Huber, G.W.; Iborra, S.; Corma, A. Synthesis of transportation fuels from biomass: Chemistry, catalysts, and engineering. *Chem. Rev.* **2006**, *106*, 4044–4098. [[CrossRef](#)] [[PubMed](#)]
3. Li, C.; Zhao, X.; Wang, A.; Huber, G.W.; Zhang, T. Catalytic Transformation of Lignin for the Production of Chemicals and Fuels. *Chem. Rev.* **2015**, *115*, 11559–11624. [[CrossRef](#)] [[PubMed](#)]
4. Zhang, Z.; Song, J.; Han, B. Catalytic Transformation of Lignocellulose into Chemicals and Fuel Products in Ionic Liquids. *Chem. Rev.* **2017**, *117*, 6834–6880. [[CrossRef](#)]
5. Upton, B.M.; Kasko, A.M. Strategies for the conversion of lignin to high-value polymeric materials: Review and perspective. *Chem. Rev.* **2016**, *116*, 2275–2306. [[CrossRef](#)] [[PubMed](#)]
6. Zhang, Q.; Chang, J.; Wang, T.; Xu, Y. Review of biomass pyrolysis oil properties and upgrading research. *Energy Convers. Manag.* **2007**, *48*, 87–92. [[CrossRef](#)]
7. Roldugina, E.A.; Naranov, E.R.; Maximov, A.L.; Karakhanov, E.A. Hydrodeoxygenation of guaiacol as a model compound of bio-oil in methanol over mesoporous noble metal catalysts. *Appl. Catal. A: Gen.* **2018**, *553*, 24–35. [[CrossRef](#)]
8. Zhang, X.; Zhang, Q.; Wang, T.; Li, B.; Xu, Y.; Ma, L. Efficient upgrading process for production of low quality fuel from bio-oil. *Fuel* **2016**, *179*, 312–321. [[CrossRef](#)]
9. Liu, W.J.; Li, W.W.; Jiang, H.; Yu, H.Q. Fates of Chemical Elements in Biomass during Its Pyrolysis. *Chem. Rev.* **2017**, *117*, 6367–6398. [[CrossRef](#)]
10. Shu, R.; Li, R.; Lin, B.; Wang, C.; Cheng, Z.; Chen, Y. A review on the catalytic hydrodeoxygenation of lignin-derived phenolic compounds and the conversion of raw lignin to hydrocarbon liquid fuels. *Biomass Bioenergy* **2020**, *132*, 105432. [[CrossRef](#)]
11. Echeandia, S.; Pawelec, B.; Barrio, V.L.; Arias, P.L.; Cambra, J.F.; Loricera, C.V.; Fierro, J.L.G. Enhancement of phenol hydrodeoxygenation over Pd catalysts supported on mixed HY zeolite and Al₂O₃. An approach to O-removal from bio-oils. *Fuel* **2014**, *117*, 1061–1073. [[CrossRef](#)]
12. Ouedraogo, A.S.; Bhoi, P.R. Recent progress of metals supported catalysts for hydrodeoxygenation of biomass derived pyrolysis oil. *J. Clean. Prod.* **2020**, *253*, 119957. [[CrossRef](#)]
13. Saidi, M.; Samimi, F.; Karimipourfard, D.; Nimmanwudipong, T.; Gates, B.C.; Rahimpour, M.R. Upgrading of lignin-derived bio-oils by catalytic hydrodeoxygenation. *Energy Environ. Sci.* **2014**, *7*, 103–129. [[CrossRef](#)]
14. Wang, X.C.; Arai, M.; Wu, Q.; Zhang, C.; Zhao, F. Hydrodeoxygenation of lignin-derived phenolics - a review on the active sites of supported metal catalysts. *Green Chem.* **2020**, *22*, 8140–8168. [[CrossRef](#)]

15. Zhang, X.; Yan, P.; Zhao, B.; Liu, K.; Kung, M.C.; Kung, H.H.; Chen, S.; Zhang, Z.C. Selective Hydrodeoxygenation of Guaiacol to Phenolics by Ni/Anatase TiO₂ Catalyst Formed by Cross-Surface Migration of Ni and TiO₂. *ACS Catal.* **2019**, *9*, 3551–3563. [[CrossRef](#)]
16. Zhang, X.; Zhang, Q.; Chen, L.; Xu, Y.; Wang, T.; Ma, L. Effect of calcination temperature of Ni/SiO₂-ZrO₂ catalyst on its hydrodeoxygenation of guaiacol. *Cuihua Xuebao/Chin. J. Catal.* **2014**, *35*, 302–309. [[CrossRef](#)]
17. Zhang, Z.; Hu, X.; Zhang, L.; Yang, Y.; Li, Q.; Fan, H.; Liu, Q.; Wei, T.; Li, C.Z. Steam reforming of guaiacol over Ni/Al₂O₃ and Ni/SBA-15: Impacts of support on catalytic behaviors of nickel and properties of coke. *Fuel Process. Technol.* **2019**, *191*, 138–151. [[CrossRef](#)]
18. Han, G.H.; Lee, M.W.; Park, S.; Kim, H.J.; Ahn, J.P.; Seo, M.G.; Lee, K.Y. Revealing the factors determining the selectivity of guaiacol HDO reaction pathways using ZrP-supported Co and Ni catalysts. *J. Catal.* **2019**, *377*, 343–357. [[CrossRef](#)]
19. Olcese, R.N.; Bettahar, M.; Petitjean, D.; Malaman, B.; Giovannella, F.; Dufour, A. Gas-phase hydrodeoxygenation of guaiacol over Fe/SiO₂ catalyst. *Appl. Catal. B Environ.* **2012**, *115–116*, 63–73. [[CrossRef](#)]
20. Hensley, A.J.R.; Wang, Y.; McEwen, J.S. Adsorption of guaiacol on Fe(110) and Pd(111) from first principles. *Surf. Sci.* **2016**, *648*, 227–235. [[CrossRef](#)]
21. Resasco, J.; Yang, F.; Mou, T.; Wang, B.; Christopher, P.; Resasco, D.E. Relationship between Atomic Scale Structure and Reactivity of Pt Catalysts: Hydrodeoxygenation of m-Cresol over Isolated Pt Cations and Clusters. *ACS Catal.* **2020**, *10*, 595–603. [[CrossRef](#)]
22. Zhu, G.; Wu, K.; Tan, L.; Wang, W.; Huang, Y.; Liu, D.; Yang, Y. Liquid Phase Conversion of Phenols into Aromatics over Magnetic Pt/NiO-Al₂O₃@Fe₃O₄ Catalysts via a Coupling Process of Hydrodeoxygenation and Dehydrogenation. *ACS Sustain. Chem. Eng.* **2018**, *6*, 10078–10086. [[CrossRef](#)]
23. Lu, M.; Du, H.; Wei, B.; Zhu, J.; Li, M.; Shan, Y.; Song, C. Catalytic Hydrodeoxygenation of Guaiacol over Palladium Catalyst on Different Titania Supports. *Energy Fuels* **2017**, *31*, 10858–10865. [[CrossRef](#)]
24. Gutierrez, A.; Kaila, R.K.; Honkela, M.L.; Slioor, R.; Krause, A.O.I. Hydrodeoxygenation of guaiacol on noble metal catalysts. *Catal. Today* **2009**, *147*, 239–246. [[CrossRef](#)]
25. Shafaghat, H.; Sirous Rezaei, P.; Daud, W.M.A.W. Catalytic hydrogenation of phenol, cresol and guaiacol over physically mixed catalysts of Pd/C and zeolite solid acids. *RSC Adv.* **2015**, *5*, 33990–33998. [[CrossRef](#)]
26. Saleheen, M.; Verma, A.M.; Mamun, O.; Lu, J.; Heyden, A. Investigation of solvent effects on the hydrodeoxygenation of guaiacol over Ru catalysts. *Catal. Sci. Technol.* **2019**, *9*, 6253–6273. [[CrossRef](#)]
27. Mu, W.; Ben, H.; Du, X.; Zhang, X.; Hu, F.; Liu, W.; Ragauskas, A.J.; Deng, Y. Noble metal catalyzed aqueous phase hydrogenation and hydrodeoxygenation of lignin-derived pyrolysis oil and related model compounds. *Bioresour. Technol.* **2014**, *173*, 6–10. [[CrossRef](#)]
28. Fang, H.; Zheng, J.; Luo, X.; Du, J.; Roldan, A.; Leoni, S.; Yuan, Y. Product tunable behavior of carbon nanotubes-supported Ni-Fe catalysts for guaiacol hydrodeoxygenation. *Appl. Catal. A Gen.* **2017**, *529*, 20–31. [[CrossRef](#)]
29. Song, W.; Liu, Y.; Baráth, E. Synergistic effects of Ni and acid sites for hydrogenation and C–O bond cleavage of substituted phenols. *Green Chem.* **2015**, *17*, 1204–1218. [[CrossRef](#)]
30. Lai, Q.; Zhang, C.; Holles, J.H. Hydrodeoxygenation of guaiacol over Ni@Pd and Ni@Pt bimetallic overlayer catalysts. *Appl. Catal. A Gen.* **2016**, *528*, 1–13. [[CrossRef](#)]
31. Mao, J.; Zhou, J.; Xia, Z.; Wang, Z.; Xu, Z.; Xu, W.; Yan, P.; Liu, K.; Guo, X.; Zhang, Z.C. Anatase TiO₂ Activated by Gold Nanoparticles for Selective Hydrodeoxygenation of Guaiacol to Phenolics. *ACS Catal.* **2017**, *7*, 695–705. [[CrossRef](#)]
32. Wan, W.; Nie, X.; Janik, M.J.; Song, C.; Guo, X. Adsorption, Dissociation, and Spillover of Hydrogen over Au/TiO₂ Catalysts: The Effects of Cluster Size and Metal-Support Interaction from DFT. *J. Phys. Chem. C* **2018**, *122*, 17895–17916. [[CrossRef](#)]
33. Qu, Y.; Zhou, W.; Ren, Z.; Du, S.; Meng, X.; Tian, G.; Pan, K.; Wang, G.; Fu, H. Facile preparation of porous NiTiO₃ nanorods with enhanced visible-light-driven photocatalytic performance. *J. Mater. Chem.* **2012**, *22*, 16471–16476. [[CrossRef](#)]
34. Yang, J.; Mou, C.Y. Ordered mesoporous Au/TiO₂ nanospheres for solvent-free visible-light-driven plasmonic oxidative coupling reactions of amines. *Appl. Catal. B Environ.* **2018**, *231*, 283–291. [[CrossRef](#)]
35. Baraton, M.I.; Busca, G.; Prieto, M.C.; Ricchiardi, G.; Escibano, V.S. On the vibrational spectra and structure of fero3 and of the ilmenite-type compounds CoTiO₃ and NiTiO₃. *J. Solid State Chem.* **1994**, *112*, 9–14. [[CrossRef](#)]
36. Chellasamy, V.; Thangadurai, P. Structural and electrochemical investigations of nanostructured NiTiO₃ in acidic environment. *Front. Mater. Sci.* **2017**, *11*, 162–170. [[CrossRef](#)]
37. Pham, T.T.; Kang, S.G.; Shin, E.W. Optical and structural properties of Mo-doped NiTiO₃ materials synthesized via modified Pechini methods. *Appl. Surf. Sci.* **2017**, *411*, 18–26. [[CrossRef](#)]
38. Daza, L.; Pawelec, B.; Anderson, J.A.; Fierro, J.L.G. Relationship between reduced nickel and activity for benzene hydrogenation on Ni-USY zeolite catalysts. *Appl. Catal. A Gen.* **1992**, *87*, 145–156. [[CrossRef](#)]
39. Hadjiivanov, K.; Mihaylov, M.; Klissurski, D.; Stefanov, P.; Abadjieva, N.; Vassileva, E.; Mintchev, L. Characterization of Ni/SiO₂ catalysts prepared by successive deposition and reduction of Ni²⁺ ions. *J. Catal.* **1999**, *185*, 314–323. [[CrossRef](#)]
40. Kordouli, E.; Pawelec, B.; Kordulis, C.; Lycourghiotis, A.; Fierro, J.L.G. Hydrodeoxygenation of phenol on bifunctional Ni-based catalysts: Effects of Mo promotion and support. *Appl. Catal. B Environ.* **2018**, *238*, 147–160. [[CrossRef](#)]
41. Hadjiivanov, K.; Knözinger, H.; Mihaylov, M. FTIR study of CO adsorption on Ni-ZSM-5. *J. Phys. Chem. B* **2002**, *106*, 2618–2624. [[CrossRef](#)]

42. Mirodatos, C.; Praliaud, H.; Primet, M. Deactivation of nickel-based catalysts during CO methanation and disproportionation. *J. Catal.* **1987**, *107*, 275–287. [[CrossRef](#)]
43. Griffin, M.B.; Baddour, F.G.; Habas, S.E.; Nash, C.P.; Ruddy, D.A.; Schaidle, J.A. An investigation into support cooperativity for the deoxygenation of guaiacol over nanoparticle Ni and Rh₂P. *Catal. Sci. Technol.* **2017**, *7*, 2954–2966. [[CrossRef](#)]
44. Selvaraj, M.; Shanthi, K.; Maheswari, R.; Ramanathan, A. Hydrodeoxygenation of guaiacol over MoO₃-NiO/mesoporous silicates: Effect of incorporated heteroatom. *Energy Fuels* **2014**, *28*, 2598–2607. [[CrossRef](#)]
45. Zhang, X.; Wang, T.; Ma, L.; Zhang, Q.; Yu, Y.; Liu, Q. Characterization and catalytic properties of Ni and NiCu catalysts supported on ZrO₂-SiO₂ for guaiacol hydrodeoxygenation. *Catal. Commun.* **2013**, *33*, 15–19. [[CrossRef](#)]